

# Dispersive modeling of breaking waves on a slope

Jihwan Kim<sup>a</sup>, Geir K. Pedersen<sup>a</sup>, Finn Løvholt<sup>a,b</sup>, Randall J. LeVeque<sup>c</sup>

<sup>a</sup>*University of Oslo, Department of Mathematics, Oslo, Norway*

<sup>b</sup>*Norwegian Geotechnical Institute, Oslo, Norway*

<sup>c</sup>*University of Washington, Department of Applied Mathematics, Seattle, USA*

---

## Abstract

The nonlinear shallow water model is widely used in the study of tsunami propagations, but an increasing number of studies are dedicated to the dispersion dynamics of tsunamis. If the wave dispersion becomes important, Boussinesq-type models are often used. In this work, an operational Boussinesq solver, BOUSSCLAW, is introduced for modeling fully non-linear dispersive tsunami propagation, taking into account inundation. In the BOUSSCLAW model, Boussinesq equations from the literature, based on the depth-averaged velocity and with enhanced dispersion properties, are implemented using a hybrid of the finite volume and finite difference methods. In order to validate BOUSSCLAW, numerical results are compared to the analytical solutions and laboratory experiments. Furthermore, the wave steepening and breaking motion is carefully scrutinized, and we demonstrate that the point of wave breaking may be wrongly identified in many of the commonly used Boussinesq models.

*Keywords:* Breaking wave, Boussinesq equation, finite volume method

---

## 1. Introduction

Tsunamis are often considered as long waves compared to the water depth, and long-wave models are consequently widely used in the study of their propagation and inundation. Through the use of numerical shock capturing techniques  
5 for modeling the nearshore bore formation of the tsunami, *nonlinear shallow water* (NLSW) models did become the standard model for modeling tsunami

propagation and run-up, see e.g. (Titov and Synolakis, 1995; Imamura, 1996; Harig et al., 2008; Berger et al., 2011).

The NLSW models do not incorporate frequency dispersion, which may be  
 10 included by ascending in the hierarchy of long wave expansion to the Boussinesq  
 type equations. Numerical models based on Boussinesq type equations have  
 been used for idealized studies of wave processes since 1966 (Peregrine, 1966) and  
 additionally to simpler problems in coastal engineering in the following decades  
 (Brocchini, 2013). However, the accumulated effect of the frequency dispersion  
 15 for the wave propagation over the open sea is a function of propagation time  
 and the shape of the disturbance (Glimsdal et al., 2013), and may become  
 important for some tsunamis, in particular for landslide sources (Løvholt et al.,  
 2015). Dispersion may further be of importance, in combination with non-  
 linear effects, for the evolution of undular bores for tsunamis (Glimsdal et al.,  
 20 2013; Grue et al., 2008; Løvholt et al., 2008; Behrens and Dias, 2015). In  
 the last decades we have seen a development on long wave expansions and  
 their numerical formulations. In the 1990s the modeling with Boussinesq type  
 equations were vitalized by new formulations, in particular those of Madsen  
 and Sørensen (1992) and Nwogu (1993) which displayed improved dispersion  
 25 properties in comparison to the standard formulation of Peregrine (1967). **A  
 few more lines here**

Boussinesq-type equations differ in mathematical structure from the NLSW  
 equations and do not inherit characteristics in the same simple form. Hence,  
 other strategies have been attempted for inclusion of wave breaking and post-  
 30 breaking motion in Boussinesq models. Schäffer et al. (1993) employed the  
 concept of the *surface roller*, first proposed by Svendsen (1984), which is vol-  
 ume of water passively riding at the bore front. Another way of incorporating  
 the breaking that was suggested by Kennedy et al. (2000) who included dif-  
 fusive terms in the momentum equation which was activated and deactivated  
 35 as a steepness measure crosses thresholds. The original steepness measure was  
 the temporal rate of surface elevation corresponding to a very steep solitary  
 wave. Later, Lynett (2006) investigated a variety of steepness measures and

then identified that the surface steepness provides the least sensitive breaking threshold. Løvholt et al. (2013) similarly employed a diffusive model including  
40 transport terms, but pointed out that breaking wave Boussinesq models were prone to instabilities. Tissier et al. (2012) suggested a breaking decision model based on the surface roller, the maximal front angle and the Froude number. An alternative non-linear diffusive ad-hoc breaking term was suggested Matsuyama et al. (2007), based on their large scale experiments of the wave propagation of  
45 undular bores on various slope angles.

However, there is a natural desire to exploit the efficient and well established shock capturing framework for NLSW models also in a dispersive context. Hence, recently developed of operational Boussinesq models are often based on hybrid numerical techniques such as use of approximate Riemann solvers combined with TVD limiters for the conserved variables, and finite differences for  
50 additional higher order terms (Erduran et al., 2005; Kim et al., 2009; Shi et al., 2012). Among other models, this have led to the popular FUNWAVE-TVD and COULWAVE-TVD applications. For instance in Shi et al. (2012), Boussinesq terms are switched off the near-shore region where large amplitude-to-depth-  
55 ratios occur, implying that only NLSW terms remain in the shallowest region. This allows for a relatively robust treatment of the modeling of the post breaking phase. To this end, the  $A/h = 0.8$  threshold suggested by (Shi et al., 2012) based on the Froude similarity analysis by Tonelli and Petti (2009), have in many ways become the standard for incorporating breaking in a feasible and  
60 practical way.

In this paper, we present a new hybrid Boussinesq type model BOUSSCLAW, of similar mould as FUNWAVE-TVD and COULWAVE-TVD. The emphasis is twofold. First, to present a careful validation of the model, both towards laboratory experiments and more general reference models. Second, we use the  
65 new model in comparison with a full potential reference model to explore how accurate the Boussinesq models can represent the wave evolution until the point of breaking. In the present example, we are finally able to demonstrate that Boussinesq models may be employed to accurately model the near shore tsunami

propagation beyond the standard  $A/h = 0.8$  threshold depth. Conversely, we  
70 find that the use of the standard  $A/h = 0.8$  threshold depth invokes a too early  
formation of a breaking bore. This points out that that the breaking criteria  
employed so far lacks generality.

This paper is organized as follows: In Section 2, the base model for the wave  
equations is given and the numerical scheme is outlined, including a von Neuman  
75 stability analysis. Sections 3 compares results from the BOUSSCLAW with the  
analytic solutions and laboratory experiments. Section 3.4 discusses the wave  
steepening and using a Boundary Integral Method (BIM) for solving the full  
potential equations. In Section 4.1, we compare these results of pre-breaking  
evolution with Boussinesq type models.

## 80 2. Model Description

Boussinesq-type equations include non-hydrostatic pressure in an approxi-  
mate way treat short waves more accurately than the shallow water equations.  
The Boussinesq-type wave models have been derived on the assumption that  
 $\mathcal{O}(\epsilon)$  and  $\mathcal{O}(\mu)$  terms are small, where  $\epsilon$  and  $\mu$  denote the ratio of wave am-  
85 plitude to depth and the ratio of depth to wavelength respectively. Various  
models have been suggested, and the papers of Peregrine (1967), Madsen and  
Sørensen (1992), Nwogu (1993), Lynett et al. (2002), and Wei and Kirby (1995)  
are representative examples.

In this work, a new numerical model, called BOUSSCLAW, is introduced. It is  
90 an extension of GEOCLAW (Clawpack Development Team, 2016), and solves the  
Boussinesq-type equations derived by Schäffer et al. (1993). The BOUSSCLAW  
model is a hybrid of the finite volume and finite difference solvers with the frac-  
tional step technique. The GEOCLAW software is a part of CLAWPACK (Claw-  
pack Development Team, 2016) developed mainly by LeVeque (1997), George  
95 (2008) and Berger et al. (2011), which is designed to solve the nonlinear shallow  
water equations.

## 2.1. BOUSSCLAW - a new long wave model for tsunami propagation and run-up

### 2.1.1. Boussinesq-type equations

Schäffer et al. (1993) derived Boussinesq-type equations with an addition of a Padé approximation of the linear dispersion relation. The equations read

$$H_t + (Hu)_x = 0, \quad (1)$$

$$(1 - D)[(Hu)_t] + \left(Hu^2 + \frac{g}{2}H^2\right)_x - gHh_x - Bgh^2(h\eta_x)_{xx} = 0, \quad (2)$$

where the operator  $D$  is defined as

$$D(w) = \left(B + \frac{1}{2}\right)h^2w_{xx} - \frac{1}{6}h^3\left(\frac{w}{h}\right)_{xx}, \quad (3)$$

for any  $w(x, t)$ . In the above equations  $H(x, t)$  and  $u(x, t)$  are the total flow  
100 depth and the depth averaged velocity of the water, respectively,  $h(x)$  is the still  
water depth,  $\eta(x, t)$  is the surface elevation, and thus  $H(x, t) = h(x) + \eta(x, t)$ .  
Moreover,  $g$  is the acceleration of gravity, and  $B$  is a dispersion parameter.  
Madsen and Sørensen (1992) have chosen the parameter  $B = 1/15$  from a  
Padé expansion of the linear dispersion analysis. When  $B = 0$ , this set of the  
105 Boussinesq-type equations approximately reduces to that of Peregrine (1967)  
as the linear dispersion relations are identical. However, unlike Peregrine's mo-  
mentum equation the hydrostatic parts of (2) are written in a conservative  
form. Moreover, some nonlinearity is introduced in the dispersion term for con-  
venience. Even though (1), (2) and (3) do not constitute a fully nonlinear set  
110 of Boussinesq equations, they do describe shoaling of solitary waves markedly  
better than, for instance, the Peregrine equations, as will be demonstrated in  
section 4.1.

The BOUSSCLAW model solves the Boussinesq-type equations (1) and (2)  
numerically with a hybrid combination of the finite volume and finite difference  
115 methods that will be explained in a moment. There have been several studies  
of this type of hybrid schemes. For example, see Tissier et al. (2011), Shi et al.  
(2012) and Dutykh et al. (2013).

To facilitate a fractional step method, as outlined below, we move the hy-  
drostatic terms of (2) inside the  $(1 - D)$  operator, while balancing with extra

terms in the  $\Psi$ , to obtain

$$(1 - D)[(Hu)_t + \left(Hu^2 + \frac{g}{2}H^2\right)_x - gHh_x] = -\Psi(x, t), \quad (4)$$

where

$$\begin{aligned} \Psi(x, t) = & \left(B + \frac{1}{2}\right) h^2 ((Hu^2)_x + gH\eta_x)_{xx} \\ & - \frac{1}{6} h^3 \left(\frac{(Hu^2)_x + gH\eta_x}{h}\right)_{xx} - Bgh^2 (h\eta_x)_{xx}. \end{aligned} \quad (5)$$

### 2.1.2. Numerical scheme

The equations (1) and (4) are written in a form that conserves momentum to leading order in  $\mu$ , but with the  $\Psi$  term as a pseudo source. Such equations may be solved by a *fractional step method* as described in LeVeque (2002), for instance. First, it is observed that (4) may be formally rewritten as

$$(Hu)_t = - \left\{ \left(Hu^2 + \frac{g}{2}H^2\right)_x - gHh_x \right\} - (1 - D)^{-1}\Psi(x, t), \quad (6)$$

At the first stage of the hybrid scheme, we integrate  $Hu$  over a time step taking into account all hydrostatic terms, namely those within the braces on the right hand side, and omitting the source terms involving  $\Psi$ . When this is combined with the continuity equation (1) this simply corresponds to advancing the shallow water equations one time step forward. To this end we employ GEOCLAW, a high-order accurate finite volume solver for the shallow water equations with adaptive mesh refinements.

In the second stage, we retain the new  $H$  value, but integrate  $Hu$  (essentially being the momentum density) further from the first stage by solving

$$(1 - D)[(Hu)_t] = -\Psi. \quad (7)$$

Since the differential operator  $D$  contains spatial derivatives, a systems of difference equations must then be solved.

The spatial and time discretization should be carefully chosen for the stability of the second stage. In our numerical scheme, the second order centered scheme is used for the spatial discretization, and a four stage Runge-Kutta

method is used for the time integration. The von Neumann stability analysis of this numerical scheme is outlined in Appendix A.

Suppose the spatial domain is divided into  $n$  grid cells with the spatial grid size  $\Delta x$ . Arrays of nodal values for flow depth and  $Hu$ , respectively, are defined as

$$\mathbf{H} = (H_1, H_2, \dots, H_n)^T,$$

$$\mathbf{M} = (H_1 u_1, H_2 u_2, \dots, H_n u_n)^T.$$

With time increment  $\Delta t$  the fourth order Runge-Kutta scheme can be written as follows,

$$\mathbf{M}^1 = \mathbf{M}, \quad \mathbf{M}^2 = \mathbf{M} + \frac{\Delta t}{2} \mathbf{S}^1, \quad \mathbf{M}^3 = \mathbf{M} + \frac{\Delta t}{2} \mathbf{S}^2, \quad \mathbf{M}^4 = \mathbf{M} + \Delta t \mathbf{S}^3, \quad (8)$$

where  $\mathbf{M}^k$  are intermediate value arrays and  $\mathbf{S}^k$  are correspondingly arrays for the time derivatives of  $Hu$ , obtained by solving

$$(I - \bar{D})\mathbf{S}^k = -\bar{\Psi}(\mathbf{H}, \mathbf{M}^k), \quad \text{for } k = 1, \dots, 4. \quad (9)$$

Here  $\bar{\Psi}$  and  $\bar{D}$  represent centered spatial discretizations for the term  $\Psi$  and the operator  $D$ , respectively. These are given explicitly below. Finally the value of  $\mathbf{M}$  at the new time level is obtained by

$$\mathbf{M}^+ = \mathbf{M} + \frac{\Delta t}{6} [\mathbf{S}^1 + 2\mathbf{S}^2 + 2\mathbf{S}^3 + \mathbf{S}^4]. \quad (10)$$

In (9),  $\bar{D}$  is a tri-diagonal  $n \times n$  matrix with elements

$$\bar{D}_{i,i-1} = \frac{1}{\Delta x^2} \left[ \left( B + \frac{1}{2} \right) h_i^2 - \frac{1}{6} \frac{h_i^3}{h_{i-1}} \right],$$

$$\bar{D}_{i,i} = \frac{1}{\Delta x^2} \left( -2B - \frac{2}{3} \right) h_i^2,$$

$$\bar{D}_{i,i+1} = \frac{1}{\Delta x^2} \left[ \left( B + \frac{1}{2} \right) h_i^2 - \frac{1}{6} \frac{h_i^3}{h_{i+1}} \right].$$

Correspondingly, the  $i$ -th element of  $\Psi(\bar{\mathbf{H}}, \mathbf{q})$  is

$$\begin{aligned}\bar{\Psi}_i = & \left( B + \frac{1}{2} \right) \frac{h_i^2}{2\Delta x^3} \left[ \left( \frac{M_{i+2}^2}{H_{i+2}} - 2\frac{M_{i+1}^2}{H_{i+1}} + 2\frac{M_{i-1}^2}{H_{i-1}} - \frac{M_{i-2}^2}{H_{i-2}} \right) \right. \\ & \left. + g(H_{i+1}(\eta_{i+2} - \eta_i) - 2H_i(\eta_{i+1} - \eta_{i-1}) + H_{i-1}(\eta_i - \eta_{i-2})) \right] \\ & - \frac{1}{6} \frac{h_i^3}{2\Delta x^3} \left[ \frac{M_{i+2}^2/H_{i+2} - M_i^2/H_i}{H_{i+1}} - 2\frac{M_{i+1}^2/H_{i+1} - M_{i-1}^2/H_{i-1}}{h_i} \right. \\ & \left. + \frac{M_i^2/H_i - M_{i-2}^2/H_{i-2}}{H_{i-1}} \right. \\ & \left. + g \left( \frac{H_{i+1}(\eta_{i+2} - \eta_i)}{H_{i+1}} - 2\frac{H_i(\eta_{i+1} - \eta_{i-1})}{h_i} + \frac{H_{i-1}(\eta_i - \eta_{i-2})}{H_{i-1}} \right) \right] \\ & - \frac{Bgh_i^2}{2\Delta x^3} (H_{i+1}(\eta_{i+2} - \eta_i) - 2H_i(\eta_{i+1} - \eta_{i-1}) + H_{i-1}(\eta_i - \eta_{i-2})),\end{aligned}$$

for  $i = 1, 2, \dots, n$ .

### 2.1.3. Additional numerical features

135 Following Shi et al. (2012) we may catch wave breaking in a heuristic fashion through invocation of a threshold  $\epsilon_B := \eta/h = 0.8$  in BOUSSCLAW. When the threshold is reached, the wave breaking is supposed to be initiated, and the dispersive terms are suppressed. At the breaking, the set of equations is locally switched to the shallow water equations for the corresponding wave packet, and  
140 the trailing waves are solved with the Boussinesq equations if the thresholds are not reached.

G: wave packet is too loose. Must specify.

When a wave reaches the coastline, the coastline changes in time as the wave runs up the slope and recedes eventually. For the numerical simulations, it has been a challenge to compute the inundation correctly. At the coastline,  
145 BOUSSCLAW switches to the NLSW solver of the GEOCLAW software, which can handle wet and dry states with the depth positivity property. Details can be found in George (2008).

RJL: I modified this sentence, is this correct?

Friction terms are important for inundation on gentle slopes. For example, the Figure 7 shows that the run-up height is much reduced by the friction terms.



BOUSSCLAW uses the Manning-type frictions as follows,

$$f_D = -\frac{gC_d^2 u |u|}{H^{5/3}},$$

where  $C_d$  is a Manning drag coefficient. Another parameter  $d^*$  needs to be chosen so that the water depth is set to  $H = 0$  if the water depth is smaller than this threshold,  $H < d^*$ . Antuono et al. (2012) derived an approximate solution of the shoreline for the shallow water equations with the Chezy friction, and studied the effect of the frictional coefficient and the water depth tolerance. In this work, the parameter  $d^*$  is set to  $10^{-4}$ .

## 2.2. Models for comparison

The performance of the Boussinesq model presented here is assessed by comparison with numerical results from a full potential flow model which is described in Løvholt et al. (2013) and references therein. The model is based on a boundary integral technique and is run with fully nonlinear solitary wave solutions as initial conditions. During shoaling and breaking this model can describe the evolution of a plunger, but breaks down when the plunger reaches the free surface. Hence, the potential flow results are used to determine the point of breaking due to shoaling and to evaluate the evolution of amplitude and wave shape of the current model until this point. Below we refer to the full potential model as the BIM (Boundary Integral Method) model.

Comparison with a pre-existing, fully nonlinear Boussinesq model is facilitated by the application of a Lagrangian model, described in Løvholt et al. (2013). Apart from the use of Lagrangian coordinates the equations employed in this model are similar to (1) and (2). They differ only concerning the nonlinearities in the dispersion terms and that the dispersion optimization terms are added in a fully nonlinear fashion. Presently, the Lagrangian model has no established bore capturing facility and is hence valid only to the point of breaking. Results from this model will be referred to as 'Serre', even though the dispersion enhancement is invoked.

Results for the Peregrine-type Boussinesq equations are obtained by the  
175 GloBouss model. This is a dispersive tsunami propagation model which is based  
on Peregrine-type equations and discretization on a staggered grid. Further  
details are found in Løvholt et al. (2008).

For comparison also the version 2.1 of the FUNWAVE-TVD model by Shi  
et al. (2012) is used. The FUNWAVE-TVD model shares important features  
180 with BOUSSCLAW, employing a hybrid of the finite volume and finite difference  
scheme to solve the fully non-linear higher order dispersive Boussinesq model  
numerically. While we refer to Shi et al. (2012) for details, we briefly note  
that FUNWAVE-TVD is based the fully nonlinear Boussinesq equations of Chen  
(2006). The numerical spatial representation in FUNWAVE-TVD is MUSCL  
185 TVD scheme to discretize for the flux and first order terms, whereas a cen-  
tral finite difference scheme Wei et al. (1995a) is utilized for the higher order  
momentum terms. A Runge-Kutta scheme is employed for the time stepping.

### 3. Numerical Tests

#### 3.1. Solitary wave propagation

In order to validate the numerical approach a solitary wave propagation  
is tested on a constant water depth. For the initial conditions, the analytic  
solitary wave solution of the Serre's equations is used since analytic solutions  
are unknown for the set (1) and (2). Solitary wave solutions to Serre's equations  
are given as

$$\begin{aligned}\eta(x, t) &= A \operatorname{sech}^2(\kappa(x - ct)), \\ u(x, t) &= c \frac{\eta(x, t)}{h},\end{aligned}\tag{11}$$

where

$$\kappa = \frac{\sqrt{3h}}{2A\sqrt{A+h}}, \quad \text{and} \quad c = \sqrt{g(A+h)}.\tag{12}$$

190 In this expression,  $A$  and  $h$  are constants which represent the wave amplitude  
and the undisturbed water depth respectively.

In Figure 1, snapshots from the BOUSSCLAW simulation are shown at  $t = 0, 4, 8$  and  $12$  with  $\Delta x = 0.1$ . For the initial conditions, the solution (11) is used with  $A = 0.2$ ,  $h = 1$  and  $g = 9.81$ . The computational results are in good agreement with the analytic solutions concerning height, shape and propagation speed. The amplitudes decreases very gently as the wave propagates.

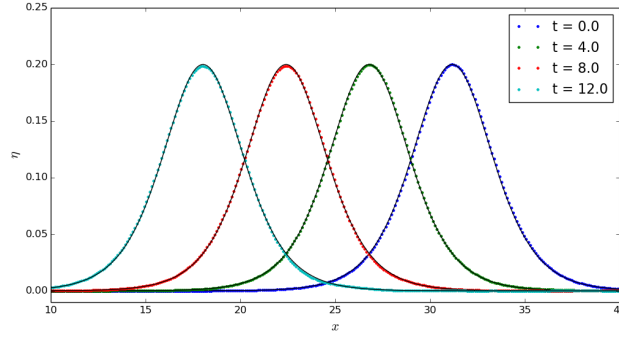


Figure 1: Snapshot of the analytic and computed solitary wave at  $t = 0, 4, 8$  and  $12$  with  $A/h = 0.2$ . The wave propagates from right to left, and the analytic solutions are black solid lines.

The wave energies for the shallow water equations and the Boussinesq equations are  $E_0$  and  $E_0 + E_1$ , respectively, where

$$E_0 = \frac{1}{2} (g\eta^2 + H\bar{u}^2), \quad (13)$$

$$E_1 = \frac{1}{6} H^3 \bar{u}_x^2 + \frac{1}{2} H^2 h_x \bar{u} \bar{u}_x + \frac{1}{2} H h_x^2 \bar{u}^2. \quad (14)$$

Details are given in Madsen et al. (1997) and Appendix B.

In Figure 2a, the energy of the solitary wave is shown with  $A/h = 0.2$  and  $\Delta x = 0.2$ . There are fluctuations both in the potential and kinetic energy that is evident when we zoom in, and the total energy decreases showing that the numerical procedure has dissipation. In Figure 2b, the relative error of the energy at  $t = 10$ ,

$$Error = \frac{|E_{t=0} - E_{t=10}|}{|E_{t=0}|},$$

RJL: Is it possible to increase the fontsize in labels of Figure 2b?

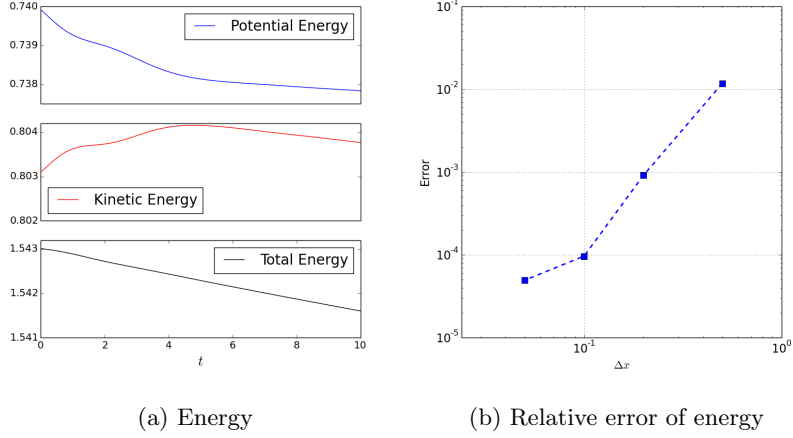


Figure 2: The energy of a solitary wave with  $\Delta x = 0.2$  (left), and log-log plot of relative error at  $t = 10$  for  $\Delta x = 0.05, 0.1, 0.2$  and  $0.5$  (right).

is shown for different  $\Delta x$ . For a solitary wave on a constant depth, the energy dissipation decreases with the grid increments.

### 3.2. Waves on a composite slope

A physical model was constructed at the Coastal Hydraulic Laboratory of the U.S. Army Corps of Engineers in order to address beach erosion and severe flooding problems Briggs et al. (1995). The model beach consists of three piecewise linear slopes of 1:53, 1:150, and 1:13 with a vertical wall at the shoreline as shown in Figure 3. In the laboratory, the wavemaker was located at 23.23 m. The gauge data from three cases are provided where the ratio  $A/h$  is equal to 0.038, 0.259 and 0.681 with  $h = 21.8$  cm.

The second case with  $A/h = 0.259$  has been compared with the numerical tests which employed 400 grid points. To specify the incoming wave from the left boundary, the data at Gauge 4 were used for the wave height, and the corresponding velocity (11) was applied.

In Figure 4, water surface elevations at gauges 5, 7 and 8 are shown. The simulated waves are in good agreement with the laboratory measurements. For the reflected waves, larger discrepancies are observed. The increased discrep-

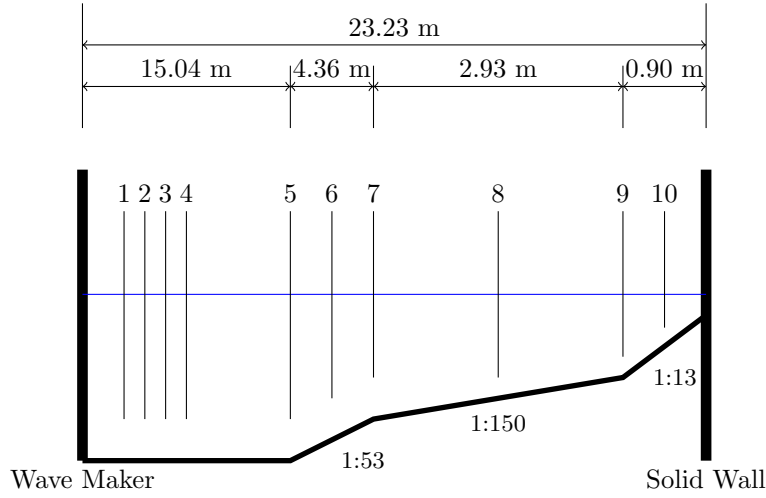


Figure 3: A sketch of the water tank

215 ancy occurs because the full interaction between the wave and the wall at the  
 right boundary is less accurately captured. Friction forces influence the wave  
 evolution along the shallow region near the right wall, but we have not included  
 these in the present numerical simulation. A better fit may possibly be obtained  
 by incorporating friction, however, tuning the friction models is not the scope  
 220 of this work.

### 3.3. Runup on a steep slope

On a  $10^\circ$  slope an incident solitary wave of amplitude  $A/h = 0.3$  will not  
 break until the end of the draw-down phase Grilli et al. (1997). Still, this may  
 be a challenging task for Boussinesq type models (Løvholt et al., 2013). Runup  
 225 on a  $10^\circ$  was investigated experimentally by Pedersen et al. (2013) who found  
 a theoretical overshoot of roughly 20% in the maximum runup height. This  
 was allotted to the viscous boundary layer on the beach and capillary effects.  
 Moreover, the measurements showed that the boundary layer flow during runup  
 was mostly laminar, albeit indications of transition was observed in the upper  
 230 part of the swash tongue close to flow reversal. Hence, it is not appropriate to  
 employ a manning friction term and we compare the models without any bed

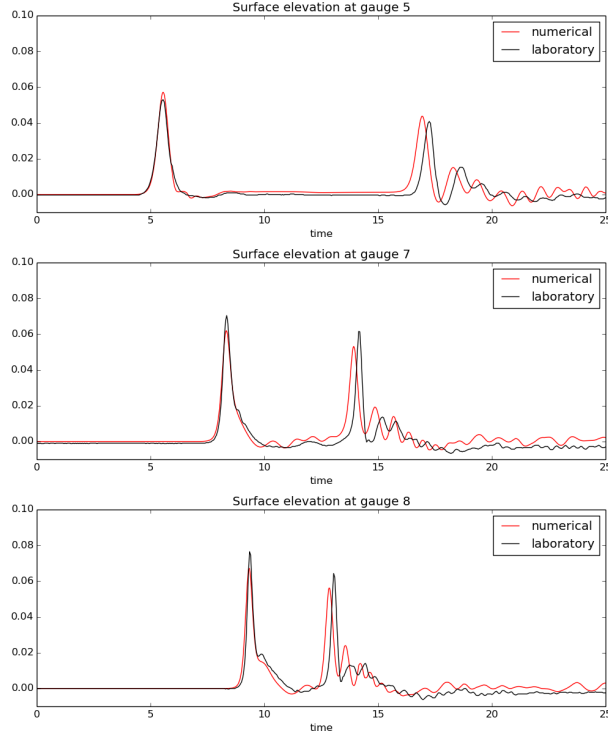


Figure 4: Water surface elevation at gauges 5,7 and 8 for  $A/h = 0.269$  case.

friction, while leaving the experiments out.

### 3.4. Comparison with experiments on a breaking wave

Synolakis (1987) performed a series of laboratory experiments for the run-  
 235 up of solitary waves on uniform slopes. Here, we are interested in the breaking  
 cases. One such example in Synolakis (1987) is a solitary wave of amplitude  
 $A/h = 0.28$  approaching a slope of 1 : 19.85. In Figure 5, the initial set-up for  
 a test is shown.

The set-up of the wave tank in the simulations follows the laboratory exper-  
 240 iments by Synolakis (1987). The bathymetry of the wave tank is composed of a  
 horizontal bottom and a uniform slope as shown in Figure 5. A solitary wave of  
 amplitude  $A/h = 0.28$  is generated at the right end of the tank and propagates  
 leftwards to the beach.

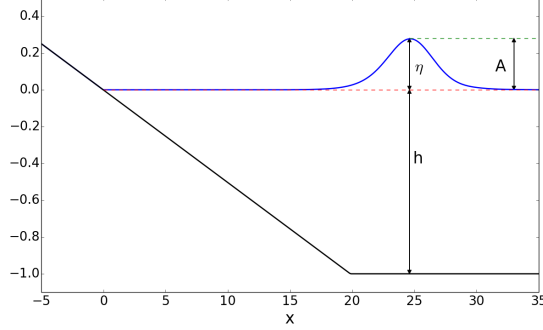


Figure 5: Set-up of a numerical test for Synolakis' experiments.

We present the results using the non-dimensional time  $t^* = t\sqrt{h/g}$  and non-dimensional space  $x^* = x/h$ . In the following, we drop the asterisks in the presentation of the results. In Synolakis (1987),  $t = 0$  was defined as when the wave crest was a non-dimensional distance,  $L$ , from the toe of the slope, where

$$L = \sqrt{\frac{4A}{3h}} \operatorname{arccosh} \left( \frac{1}{0.05} \right).$$

However, at  $t = 0$ , the solitary wave has an elevation of 5% of its maximum at the toe of the beach, meaning that the slope has started to interact with the solitary wave. To avoid any such interaction obscuring our analysis, we instead place the initial solitary wave using equation (11) at  $L + 5c$ , where  $c$  is the shallow water wave celerity. In this way, the initial solitary wave has a negligible interaction with the slope when initialized.

In Figure 6, the laboratory measurements are shown with the computational results from the BOUSSCLAW (in Boussinesq and NLSW mode) and the BIM models for  $A/h = 0.28$  and a 1 : 19.85 slope at  $t = 15$ . This is before the wave breaks and both BOUSSCLAW and the BIM model are in good agreement with the experiments.

The ratio of amplitude to depth,  $A/h$ , is about 2.01 at the break point. The potential flow model cannot be run much beyond the breaking points (until the attachment of the plunger only) and gives no information on the following bore propagation. In figure 7 we have compared the BOUSSCLAW model, with and

Also include the BoussClaw results and NLSW in fig. 6

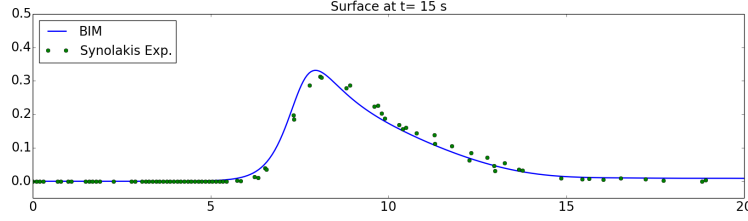


Figure 6: Comparison of the laboratory experiments and BIM at  $t=15$  with  $A/h = 0.28$  on a slope of 1 : 19.85.

without a Manning friction, with the experimental data. The agreement is good  
 260 and the introduction of bed-friction even seem to match the truncated swash  
 tongue of the experiments well. However, this may be a coincidence. Even  
 though the wave has broken and some irregular flow features are introduced  
 thereby, we have no evidence of the flow state being anywhere near turbulent,  
 which is required for a quadratic bottom resistance to be appropriate. Capillary  
 effects and experimental errors may also affect the comparison.

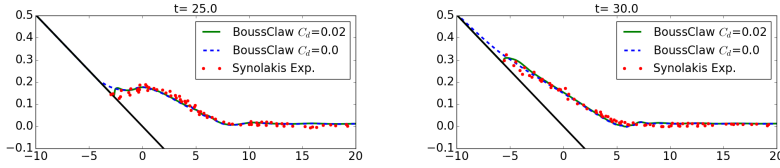


Figure 7: Comparison of experiments and BoussClaw results at  $t=25$  and  $30$ .

## 4. Shoaling and breaking phenomena

### 4.1. Pre-breaking

Wei et al. (1995b) made computation of pre-breaking solitary wave shoaling  
 with their fully nonlinear extension of Nwogu's model with full potential theory  
 270 and the weakly nonlinear version of Nwogu's model. They found that the fully  
 nonlinear Boussinesq equations were superior to those of Nwogu in the later  
 stages of the shoaling. In this subsection we will do a similar comparison for  
 our models on the 1 : 19.85 slope which was not included in the reference.



275 We use the set-up described in section 3.4 for the Boussinesq modeling of solitary waves on a slope. The BOUSSCLAW simulations are compared with those of other Boussinesq solvers, namely FUNWAVE (Shi et al., 2012), GLOBOUSS (Løvholt et al., 2010) and the Serre type formulation (Løvholt et al., 2013). As noted above, the original Serre’s equations are enhanced by adding the Schäffer et al. (1993) terms.

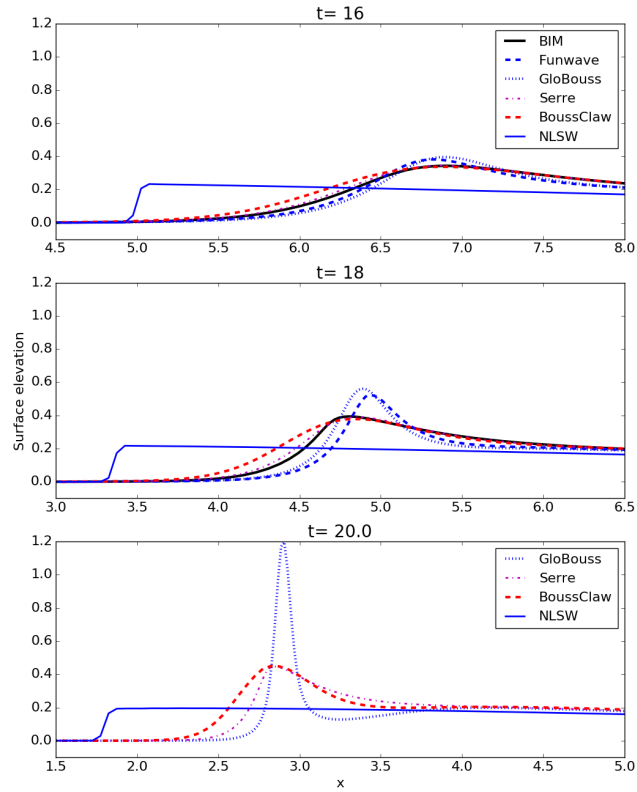


Figure 8: Snapshots of BIM, Serre, GLOBOUSS, BOUSSCLAW and FUNWAVE at  $t = 16$ , 18 and 20. The BOUSSCLAW is used with  $B=1/15$ , and the Peregrine’s form is used for GLOBOUSS.

280 In Figure 8, snapshots from different numerical models are shown at  $t = 16$ , 18 and 20. At the  $t = 20$  there are no results from the BIM model as the wave

has broken. For the BOUSSCLAW, the parameter  $B = 1/15$  is used, but the computational results are rather similar with  $B = 0$  for this case. At  $t=16$ , the computational results from the Boussinesq-type equations show similar results.

285 The NLSW model, on the other hand, has yielded a premature breaking causing a too low amplitude. Moreover, the wave celerity is also over-estimated by the hydrostatic model. At  $t=18$ , some discrepancies are observed that can be split into two groups, and GLOBOUSS and FUNWAVE are similar while the BOUSSCLAW and the Serre results are similar. The wave amplitudes computed

290 by the GLOBOUSS and FUNWAVE models, are more than 20 %larger than those from the BIM model. The wave amplitude continues to increase with GLOBOUSS simulations, and the difference from the BOUSSCLAW result becomes larger at  $t = 20$ . The results from the Serre and BOUSSCLAW models clearly more similar to those of the BIM model. Especially, the wave amplitudes are correctly

295 determined by these models. Our observations are in line with those of Wei et al. (1995b).

RJL: Why no BIM solution at  $t = 20$ ? G: could we include  $t=19.1$  instead, with the BIM in place ?

Is the figure 20% OK. The old 10 was far too small

#### 4.2. Wave breaking and run-up

In the BIM model we may identify the onset of breaking according when and where we first observe a vertical slope at the wave front. For an incident

300 amplitude of  $A/h = 0.28$  on a  $1 : 19.85$  slope breaking then starts at  $x = 4.09$ . When the crest in the BOUSSCLAW simulation reaches  $x = 4.09$  we find  $A/h = 1.97$ , the ratio of wave speed to celerity ( $u/\sqrt{gH}$ ) is 1.034 and maximum surface slope angle of  $39.1^\circ$ .

What are the height, time, etc for the BIM simulation

For an incident amplitude of  $A/h = 0.28$  and a  $1 : 19.85$  slope the BOUSS-

305 CLAW model, the threshold  $\epsilon_B = 0.8$  (see sec. 2.1.3) is reached at  $t = 14.9$  when the peak of the wave is at  $x = 8.03227$ . In the following, we explore the wave evolution with and without the application of this threshold.

In Figure 9, snapshots are shown at  $t=20, 25$ , and  $30$  of the solutions from BOUSSCLAW and NLSW with the Manning coefficient  $C_d = 0.02$ . We compared

310 the NLSW and BOUSSCLAW with  $\epsilon_B = 0.8$  and without the threshold. At  $t = 20$  the simulation with  $\epsilon_B = 0.8$  has already been in NLSW mode for 5 time units

and the difference in the wave height from the full Boussinesq simulation is significant. In fact, the threshold solution is closer to the NLSW solution. is clearly observed.

315 At  $t = 25$  and  $t = 30$ , the wave is running up the slope, and the difference in the swash tongue is relatively small. On the other hand, while BOUSSCLAW simulation with  $\epsilon_B = 0.8$  is smooth at  $t = 20$  irregularities are observed around  $x = 8$  due to the accumulated errors generated by the splicing of Boussinesq and NLSW equations.

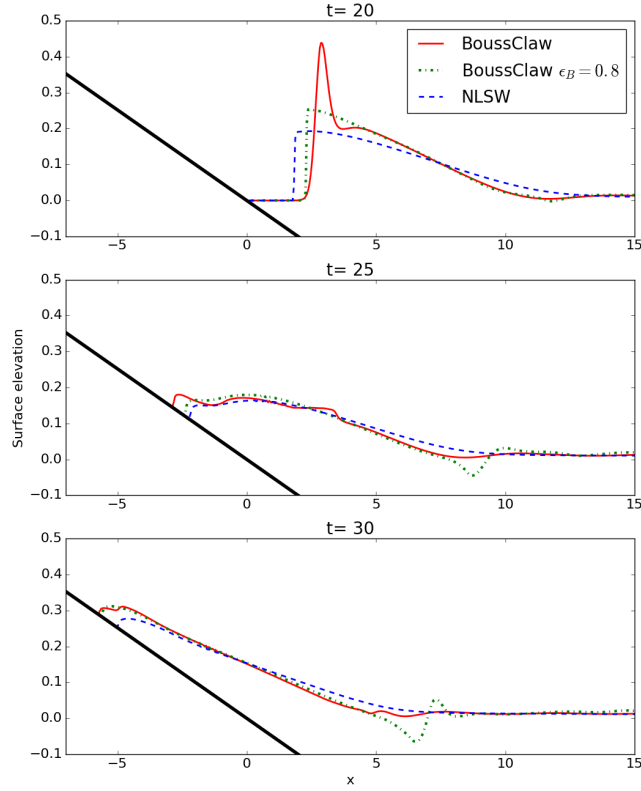


Figure 9: Comparison of BOUSSCLAW and NLSW with  $\epsilon_B = 0.8$  at  $t = 20, 25$  and  $30$ . Fiction forces have been added with  $C_d = 0.02$ .

How does  
this evolve?  
Is it seen in  
other paper  
?

Figure 10 shows the amplitude to depth ratio,  $\epsilon_B$ , as function of the crest location.

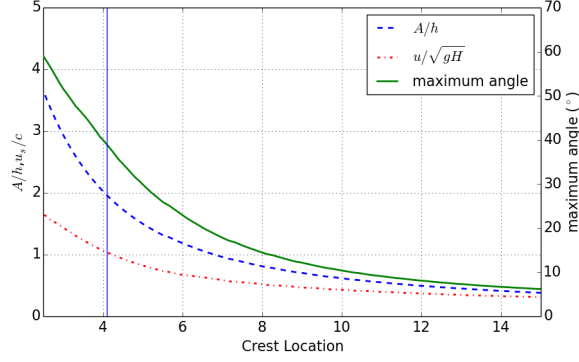


Figure 10: Plot of  $A/\eta$ ,  $u_s/c$  and maximum angle of waves vs. crest location. BIM shows the wave break at  $x = 4.09$ .

#### 4.3. Wave Energy

The wave energy is nearly conserved when the wave is smooth, but decreases as the wave breaks. The wave energy expressions for the shallow water equations and Boussinesq equations are  $E_0$  and  $E_0 + E_1$  respectively, which are given in (13) and (14).

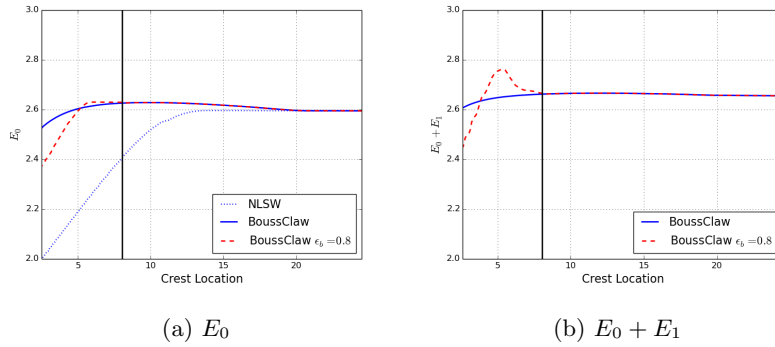


Figure 11: Energy plots of NLSW and BOUSSCLAW. The vertical line is at  $x = 8.03227$  m where  $\epsilon_B = 0.8$ , and the governing equations are switched to the NLSW from the Boussinesq equations.

In Figure 11, the wave energy  $E_0$  and  $E_0 + E_1$  are shown. The energy denotes the aggregate of the wave energy in the entire computational domain and is shown as function of the crest location. In the left panel, the energy  $E_0$  is well-preserved for the shallow water equations before the wave forms a shock, and then the energy dissipates after a shock is formed. In the right panel,  $E_0 + E_1$  is well-preserved for the BOUSSCLAW simulation during deep water propagation, but the value decreases slightly as the wave steepens near the shoreline. When the threshold  $\epsilon_B = 0.8$  is used, the energy  $E_0 + E_1$  is well-preserved as shown on the right figure before the threshold is reached. When the crest is located at  $x = 8.03227$  with  $\epsilon_B = 0.8$ , the wave energy  $E_0$  on the left figure does not decrease immediately. The energy  $E_0$  is preserved for a while, then starts to decrease as a shock is formed.

## 5. Conclusion

In the present paper we have presented a new operational Boussinesq type model, BOUSSCLAW, for modeling fully non-linear dispersive tsunami propagation, taking also into account drying-wetting during inundation and withdrawal on the beach. BOUSSCLAW resembles much used operational models such as FUNWAVE-TVD and COULWAVE-TVD, but is based on a slightly simpler and more transparent set of governing equations, and has a slightly different numerical scheme. We have tested numerical implementation towards analytical solitary wave expressions as well as laboratory experiments.

Making use of the experiments of Synolakis (1987) enabled us to constrain a set of different long wave models, including BOUSSCLAW, as well as a full potential BIM reference model. Using the BIM, we were able to explore in detail the post-breaking behaviour, and to identify the point of breaking accurately. This was useful for determining the validity of the respective long wave models. First, we found that by using standard NLSW models, the point of breaking will be located too far offshore. Boussinesq models provide the opportunity of providing a more accurate description of the near shore propagation and

RJL: Here and in the abstract, is “operational” the right word? To me this means a code that is used in practical work such at tsunami warning centers.

shoaling. However, in current practise the Boussinesq terms are often omitted near shore through the  $A/h > 0.8$  threshold criteria. As a consequence, the point of breaking may be misinterpreted also in Boussinesq type models.

In the present example, we investigated the near shore propagation over a relatively gentle shelf of  $1/19.85$  slope, and in this case the actual onset of breaking occurred for  $A/h \approx 2$ , which is significantly later than what would be predicted in any standard approach (NLSW or Boussinesq). As demonstrated in this paper, the combined effects of non-linearities and dispersion influence the solution markedly, when accumulated to the point of breaking. It is noted that the artificial effect discovered would depend on the slope, and the  $A/h = 0.8$  limited may well work better on a much gentler slope as it is primarily derived based on solitary wave evolution on constant depth. On the other hand,  $1/19.85$  slope is already quite gentle, and the offset between the reference solution and Boussinesq models using this criteria may be even more pronounced for steeper slopes.

## References

- V. V. Titov, C. E. Synolakis, Modeling of breaking and nonbreaking long-wave evolution and runup using VTCS-2, *Journal of Waterway, Port, Coastal, and Ocean Engineering* 121 (6) (1995) 308–316.
- F. Imamura, Long-wave runup models, chapter Simulation of wave-packet propagation along sloping beach by TUNAMI-code, *World Scientific* 3 (1996) 4.
- S. Harig, Chaeroni, W. S. Pranowo, J. Behrens, Tsunami simulations on several scales, *Ocean Dynamics* 58 (5) (2008) 429–440, ISSN 1616-7228.
- M. J. Berger, D. L. George, R. J. LeVeque, K. T. Mandli, The GeoClaw software for depth-averaged flows with adaptive refinement, *Adv. Water Res.* 34 (2011) 1195–1206.
- D. H. Peregrine, Calculations of the development of an undular bore, *J. Fluid Mech.* 25 (1966) 321–330.

- M. Brocchini, A reasoned overview on Boussinesq-type models: the interplay between physics, mathematics and numerics, *Proc. R. Soc.* 469 (2013) 20130496.
- 385 S. Glimsdal, G. Pedersen, C. Harbitz, F. Løvholt, Dispersion of tsunamis: does it really matter?, *Nat. Hazards Earth Syst. Sci.* 13 (2013) 1507–1526.
- F. Løvholt, G. Pedersen, C. Harbitz, S. Glimsdal, J. Kim, On the characteristics of landslide tsunamis, *Phil. Trans. R. Soc. A* 373 (2053) (2015) 20140376.
- 390 J. Grue, E. N. Pelinovsky, D. Fructus, T. Talipova, C. Kharif, Formation of undular bores and solitary waves in the Strait of Malacca caused by the 26 December 2004 Indian Ocean tsunami, *J. Geophys. Res.* 113 (2008) C05008.
- F. Løvholt, G. Pedersen, G. Gisler, Oceanic propagation of a potential tsunami from the La Palma Island, *J. Geophys. Res.* 113 (2008) C09026.
- 395 J. Behrens, F. Dias, New computational methods in tsunami science, *Phil. Trans. R. Soc. A* 373 (2053) (2015) 20140382.
- P. A. Madsen, O. R. Sørensen, A new form of the Boussinesq equations with improved linear dispersion characteristics. Part 2. A slowly-varying bathymetry, *Coastal Engineering* 18 (3) (1992) 183–204.
- 400 O. Nwogu, Alternative form of Boussinesq equations for nearshore wave propagation, *Journal of waterway, port, coastal, and ocean engineering* 119 (6) (1993) 618–638.
- D. H. Peregrine, Long waves on a beach, *Journal of Fluid Mechanics* 27 (04) (1967) 815–827.
- 405 H. A. Schäffer, P. A. Madsen, R. Deigaard, A Boussinesq model for waves breaking in shallow water, *Coastal Engineering* 20 (3) (1993) 185–202.
- I. A. Svendsen, Mass flux and undertow in a surf zone, *Coast. Eng.* 8 (1984) 347365, doi:10.1016/0378-3839(84)90030-9.

- 410 A. B. Kennedy, Q. Chen, J. T. Kirby, R. A. Dalrymple, Boussinesq modeling  
of wave transformation, breaking, and run-up. Part I: 1D., J. Waterw., Port,  
Coast., Ocean Engrg. 126 (1) (2000) 39–47.
- P. J. Lynett, Nearshore wave modeling with high-order Boussinesq-type equa-  
tions, Journal of Waterway, Port, Coastal, and Ocean Engineering 132 (5)  
(2006) 348–357.
- 415 F. Løvholt, P. Lynett, G. K. Pedersen, Simulating run-up on steep slopes with  
operational Boussinesq models; capabilities, spurious effects and instabilities,  
Nonlin. Processes Geophys. 20 (2013) 379–395.
- M. Tissier, P. Bonneton, F. Marche, F. Chazel, D. Lannes, A new approach to  
handle wave breaking in fully non-linear Boussinesq models, Coastal Engi-  
420 neering 67 (2012) 54–66.
- M. Matsuyama, M. Ikeno, T. Sakakiyama, T. Takeda, A study of tsunami wave  
fission in an undistorted experiment, Pure and Applied Geophysics 164 (2-3)  
(2007) 617–631.
- K. Erduran, S. Ilic, V. Kutija, Hybrid finite-volume finite-difference scheme for  
425 the solution of Boussinesq equations, Int. J. for Num. Meth. in Fluids 49  
(2005) 1213–1232.
- D.-H. Kim, P. Lynett, S. Socolofsky, A depth-integrated model for weakly dis-  
persive, turbulent, and rotational flows, Ocean Modelling 27 (2009) 198–214.
- F. Shi, J. T. Kirby, J. C. Harris, J. D. Geiman, S. T. Grilli, A high-order adaptive  
430 time-stepping TVD solver for Boussinesq modeling of breaking waves and  
coastal inundation, Ocean Modelling 43 (2012) 36–51.
- M. Tonelli, M. Petti, Hybrid finite volume–finite difference scheme for 2DH  
improved Boussinesq equations, Coastal Engineering 56 (5) (2009) 609–620.
- P. J. Lynett, T. R. Wu, P. L. F. Liu, Modeling wave runup with depth-integrated  
435 equations, Coastal Engineering 46 (2) (2002) 89–107.



- G. Wei, J. T. Kirby, Time-dependent numerical code for extended Boussinesq equations, *Journal of Waterway, Port, Coastal, and Ocean Engineering* 121 (5) (1995) 251–261.
- Clawpack Development Team, Clawpack software, URL <http://www.clawpack.org>, version 5.3.1, 2016.
- R. J. LeVeque, Wave propagation algorithms for multidimensional hyperbolic systems, *Journal of Computational Physics* 131 (2) (1997) 327–353.
- D. L. George, Augmented Riemann solvers for the shallow water equations over variable topography with steady states and inundation, *Journal of Computational Physics* 227 (6) (2008) 3089–3113.
- M. Tissier, P. Bonneton, F. Marche, F. Chazel, D. Lannes, Serre Green-Naghdi modelling of wave transformation breaking and run-up using a high-order finite-volume finite-difference scheme, *Coastal Engineering Proceedings* 1 (32) (2011) 13.
- D. Dutykh, T. Katsaounis, D. Mitsotakis, Finite volume methods for unidirectional dispersive wave models, *International Journal for Numerical Methods in Fluids* 71 (6) (2013) 717–736.
- R. J. LeVeque, Finite volume methods for hyperbolic problems, vol. 31, Cambridge university press, 2002.
- M. Antuono, L. Soldini, M. Brocchini, On the role of the Chezy frictional term near the shoreline, *Theoretical and Computational Fluid Dynamics* 26 (1-4) (2012) 105–116.
- Q. Chen, Fully nonlinear Boussinesq-type equations for waves and currents over porous beds, *J. of Eng. Mech., ASCE* 132 (2) (2006) 220–230.
- G. Wei, J. T. Kirby, S. T. Grilli, R. Subramanya, A fully nonlinear Boussinesq model for surface waves. Part 1. Highly nonlinear unsteady waves, *J. Fluid Mech.* 294 (1995a) 71–92.

- P. A. Madsen, O. Sørensen, H. Schäffer, Surf zone dynamics simulated by a Boussinesq type model. Part I. Model description and cross-shore motion of regular waves, Coastal Engineering 32 (4) (1997) 255–287.
- M. Briggs, C. Synolakis, U. Kanoglu, D. Green, Runup of solitary waves on a vertical wall, Costal Hydraulics Laboratory, URL <http://chl.erd.c.usace.army.mil/chl.aspx?p=s&a=Projects;36>, 1995.
- S. Grilli, I. Svendsen, R. Subramanya, Breaking Criterion and Characteristics for Solitary Waves on Slopes, J. Waterw. Port, Coastal, Ocean Eng. 123 (3) (1997) 102–112.
- G. K. Pedersen, E. Lindstrøm, A. F. Bertelsen, A. Jensen, D. Laskovski, G. Sælevik, Runup and boundary layers on sloping beaches, Physics of Fluids 25 (2013) pp. 23, doi: 10.1063/1.4773327.
- C. E. Synolakis, The runup of solitary waves, Journal of Fluid Mechanics 185 (1987) 523–545.
- F. Løvholt, G. Pedersen, S. Glimsdal, Coupling of Dispersive Tsunami Propagation and Shallow Water Coastal, Open Oceanography Journal 4 (2010) 71–82.
- G. Wei, J. T. Kirby, S. T. Grilli, R. Subramanya, et al., A fully nonlinear Boussinesq model for surface waves. Part 1. Highly nonlinear unsteady waves, Journal of Fluid Mechanics 294 (7) (1995b) 71–92.
- T. B. Benjamin, J. L. Bona, J. J. Mahony, Model equations for long waves in nonlinear dispersive systems, Philosophical Transactions of the Royal Society of London A: Mathematical, Physical and Engineering Sciences 272 (1220) (1972) 47–78.

## Appendix A. Stability of the hybrid scheme

It is difficult to analyze the numerical stability for our full Boussinesq equations. To obtain some insight in the stability of the proposed hybrid numerical

scheme, we thus consider a closely related, but simpler, equation, namely the linearized Benjamin-Bona-Mahony (BBM) equation (Benjamin et al. (1972))

$$u_t + cu_x = \frac{h^2}{6}u_{txx}, \quad (\text{A.1})$$

where  $c = \sqrt{gh}$ . This equation describes weakly dispersive, uni-directional waves in constant depth. The equation replaces the momentum equation, whereas no  
490 separate continuity equation is involved.

Following the steps of section 2.1.2, we rearrange the equation (A.1) as

$$(I - D)(u_t + cu_x) + Du_x = 0, \quad (\text{A.2})$$

where  $D = \frac{h^2}{6}\partial_x^2$ . The first step of hybrid scheme for this equation is integration of the advection equation

$$u_t + cu_x = 0, \quad (\text{A.3})$$

by the finite volume method. Then the Runge-Kutta method is applied to,

$$(1 - D)u_t + cDu_x = 0. \quad (\text{A.4})$$

which is the counterpart to (7).

If we use the centered spatial difference approximation of  $O(\Delta x^2)$  accuracy on a regular grid we may employ a standard von Neumann analysis where we calculate the growth of an harmonic mode over a single time step. Expressing  
495 the coefficients of the velocity array before the time step as  $u_j = e^{i\xi j\Delta x}$  we then replace the coefficient of  $\mathbf{M}^q$ , defined in section 2.1.2, by  $M_j^q = U_j^q = g^q e^{i\xi j\Delta x}$ , where  $q$  is 1, 2, 3, 4 or +. Correspondingly, the coefficients of the  $\mathbf{S}^k$  array, which contains auxiliary, nodal values for  $u_t$ , is expressed  $(S_j^k) = s^k e^{i\xi j\Delta x}$ .

The stability of the first step, (A.3), is assured by the standard CFL criterion

$$\frac{c\Delta t}{\Delta x} < 1.$$

If we instead solve the NLSW equations, as in BOUSSCLAW,  $c$  must be replaced by the nonlinear characteristic velocity, which may lead to a more strict criterion. However, the method employed in the first step is not suited for a von Neumann

stability analysis and we thus apply this technique to the second step only. Hence, we may put  $g^1$  to unity, but it is preferable to retain it in the calculations. The Runge-Kutta scheme for time stepping, (8), may now be expressed as

$$g^2 = g^1 + \frac{\Delta t}{2} s^1, \quad g^3 = g^1 + \frac{\Delta t}{2} s^2, \quad g^4 = g^1 + \Delta t s^3, \quad (\text{A.5})$$

The discrete version of (A.4), which is the counterpart to (9) for the BBM equation reads

$$S_j^k - \frac{h^2}{6} \frac{S_{j+1}^k - 2S_j^k + S_{j-1}^k}{\Delta x^2} = -\frac{ch^2}{6} \frac{U_{j+2}^k - 2U_{j+1}^k + 2U_{j-1}^k - U_{j-2}^k}{2\Delta x^3},$$

which, inserted the harmonic expressions, implies

$$s^k = i \frac{\gamma}{\Delta t} g^k, \quad \gamma = c\Delta t \frac{2 \sin(\xi \Delta x)(1 - \cos(\xi \Delta x))}{6\Delta x^3 h^{-2} + 2\Delta x(1 - \cos(\xi \Delta x))}, \quad (\text{A.6})$$

where the  $\Delta t$  factors are included for convenience. The assembling of the intermediate values in the Runge-Kutta procedure, (10), now yields

$$g^+ = g^1 + \frac{\Delta t}{6} [s^1 + 2s^2 + 2s^3 + s^4]. \quad (\text{A.7})$$

By combination of (A.5) and (A.6)  $s^k$  and  $g^k$ ,  $k = 1..4$  can be calculated successively and combined in (A.7) to provide the value of  $g^+$ ,

$$\begin{aligned} g^+(\gamma) &= \left(1 - \frac{1}{2}\gamma^2 + \frac{\gamma^4}{24} + \left(\frac{\gamma^3}{6} - \gamma\right)i\right) g^1 \\ |g^+(\gamma)|^2 &= \left(1 + \frac{1}{4}\gamma^4 + \frac{\gamma^8}{24^2} - \gamma^2 + \frac{\gamma^4}{12} - \frac{\gamma^6}{24} + \gamma^2 + \frac{\gamma^6}{36} - \frac{\gamma^4}{3}\right) |g^1|^2 \\ &= \left(1 - \frac{1}{72}\gamma^6 + \frac{1}{576}\gamma^8\right) |g^1|^2. \end{aligned}$$

Stability requires  $|g^+(\gamma)/g^1| < 1$  which is equivalent to  $|\gamma| < 2\sqrt{2}$ . Moreover, it is easily seen that  $\gamma < c\Delta t/\Delta x$ . Hence, a sufficient condition for stability of the second step of the hybrid scheme is

$$\frac{c\Delta t}{\Delta x} < 2\sqrt{2}.$$

This is more relaxed than the CFL condition for the advection equation (A.3).

500 Therefore, if the CFL condition is satisfied in the advection equation, the fractional step is always stable with the suggested numerical scheme.

## Appendix B. Energy estimates and dissipation

### Appendix B.1. Velocity field

To derive the energy estimates for the Boussinesq-type equations, we define the depth-averaged velocity as,

$$\bar{u} = \frac{1}{H} \int_{-h}^{\epsilon\eta} u dz.$$

Then the velocity  $u$  can be expressed as  $u = \bar{u} + \mu^2 u_1$  where

$$\int_{-h}^{\epsilon\eta} u_1 dz = 0. \quad (\text{B.1})$$

Then the kinematic boundary condition at the bottom and zero divergence implies

$$w = -h_x u - \bar{u}_x(z+h) + O(\mu^2).$$

### Appendix B.2. Energy integrals

The potential energy density per horizontal area is

$$V = \int_{-h}^{\epsilon\eta} g z dz = \frac{1}{2} \epsilon^2 g \eta^2 - \frac{1}{2} g h^2,$$

where the last term  $\frac{1}{2} g h^2$  is the equilibrium energy. The kinematic energy density has two contributions,

$$T = T_u + T_w; \quad T_u = \frac{1}{2} \epsilon^2 \int_{-h}^{\epsilon\eta} u^2 dz, \quad T_w = \frac{1}{2} \epsilon^2 \mu^2 \int_{-h}^{\epsilon\eta} w^2 dz.$$

For the horizontal part,  $T_u$  is

$$T_u = \frac{1}{2} \epsilon^2 \int_{-h}^{\epsilon\eta} u^2 dz = \frac{1}{2} \epsilon^2 \int_{-h}^{\epsilon\eta} \bar{u}^2 + 2\mu^2 \bar{u} u_1 + \mu^4 u_1^2 dz = \frac{1}{2} \epsilon^2 H \bar{u}^2 + O(\epsilon^2 \mu^4),$$

since  $\bar{u}$  is independent of  $z$  and by (B.1). Assuming  $\frac{1}{H} \int_{-h}^{\epsilon\eta} u^2 dz = \bar{u}^2$ , the vertical part is

$$\begin{aligned} T_u &= \frac{1}{2} \epsilon^2 \mu^2 \int_{-h}^{\epsilon\eta} h_x^2 u^2 + 2h_x u \bar{u}_x(z+h) + \bar{u}_x^2(z+h)^2 dz + O(\epsilon^2 \mu^4) \\ &= \frac{1}{2} \epsilon^2 \mu^2 H \left( h_x^2 \bar{u}^2 + H h_x \bar{u} \bar{u}_x + \frac{1}{3} H^2 \bar{u}_x^2 \right) + O(\epsilon^2 \mu^4). \end{aligned}$$

Thus the energy of a wave can be approximated as

$$E = \epsilon^2 (E_0 + \mu^2 E_1 + O(\mu^4))$$

where

$$\begin{aligned} E_0 &= \frac{1}{2} (g\eta^2 + H\bar{u}^2), \\ E_1 &= \frac{1}{6} H^3 \bar{u}_x^2 + \frac{1}{2} H^2 h_x \bar{u} \bar{u}_x + \frac{1}{2} H h_x^2 \bar{u}^2. \end{aligned}$$